

Surface Networks via General Covers

Niv Haim *

Nimrod Segol *

Heli Ben-Hamu

Haggai Maron

Yaron Lipman

Weizmann Institute of Science
Rehovot, Israel

Abstract

Developing deep learning techniques for geometric data is an active and fruitful research area. This paper tackles the problem of sphere-type surface learning by developing a novel surface-to-image representation. Using this representation we are able to quickly adapt successful CNN models to the surface setting.

The surface-image representation is based on a covering map from the image domain to the surface. Namely, the map wraps around the surface several times, making sure that every part of the surface is well represented in the image. Differently from previous surface-to-image representations we provide a low distortion coverage of all surface parts in a single image.

We have used the surface-to-image representation to apply standard CNN models to the problem of semantic shape segmentation and shape retrieval, achieving state of the art results in both.

1. Introduction

Adapting deep learning methods to geometric data (*e.g.*, shapes) is a promising research area that has already produced state of the art algorithms for several geometric learning tasks (*e.g.*, [27, 28, 32]).

Two prominent strategies for tackling this problem are: (i) translating the geometric data to tensors (*e.g.*, images) and using off-the-shelf convolutional neural networks (CNN) architectures and optimization techniques [32, 37, 31, 19]; and (ii) developing novel architectures and optimization techniques that are tailored to the geometric data [20, 27, 28]. The main benefit in strategy (i) is its ability to harness the *huge* algorithmic progress of neural networks for images directly to geometric data.

The goal of this paper is to devise a method to transfer geometric data from sphere-like (genus zero) surfaces to

tensor representation in a way that facilitates efficient and effective learning of such data.

Some previous attempts use projections to 2D planes, *e.g.*, by rendering the shapes [32]. Such projections are not injective and suffer from occlusions and thus often require a collection of projections for a single shape. Other methods embed the shape in an encapsulating 3D grid [37, 21]; these methods require dealing with higher dimensional tensors and are usually less robust to deformations. Other methods [31, 19] try to find low distortion 2D mappings to an image domain. In this case the intrinsic dimensionality of the data is preserved, however, these maps suffer from high distortion and/or ignore the difference in the topologies of the surface (no boundary) and the image (with boundary).

In this paper, we replace the notion of a one-to-one mapping with a *covering map*. That is, we construct a mapping from the image domain to the surface that covers the surface several times. Differently put, each part of the surface is shown several times in the image. We ask the cover to *well represent* the surface, that is, each part of the surface has at least one low distortion representation in the image. This is similar to an atlas representation of a surface but with a *single* image. Since the image domain has a boundary while a sphere-like surface does not, the covering map representation (which is locally a homeomorphism¹) requires us to think about the image domain without boundaries. We opt for a toric topology since it will make standard CNNs (in particular, convolutions) well-defined and continuous when considered as operators acting on functions defined over the surfaces [19].

The most similar method to ours is [19] that uses a specific type of covering map (generated by symmetry groups of the plane), see Figure 1 (b). However, these covering maps usually introduce extreme shrinking of parts of the surface (see *e.g.*, the head, right arm and torso in Figure 1 (b)). Second, all their coverings are identical up to rotation and translation so the image resolution is not used to cover with low distortion different parts of the surface.

*Equal contribution

¹Homeomorphism is a continuous map with a continuous inverse.

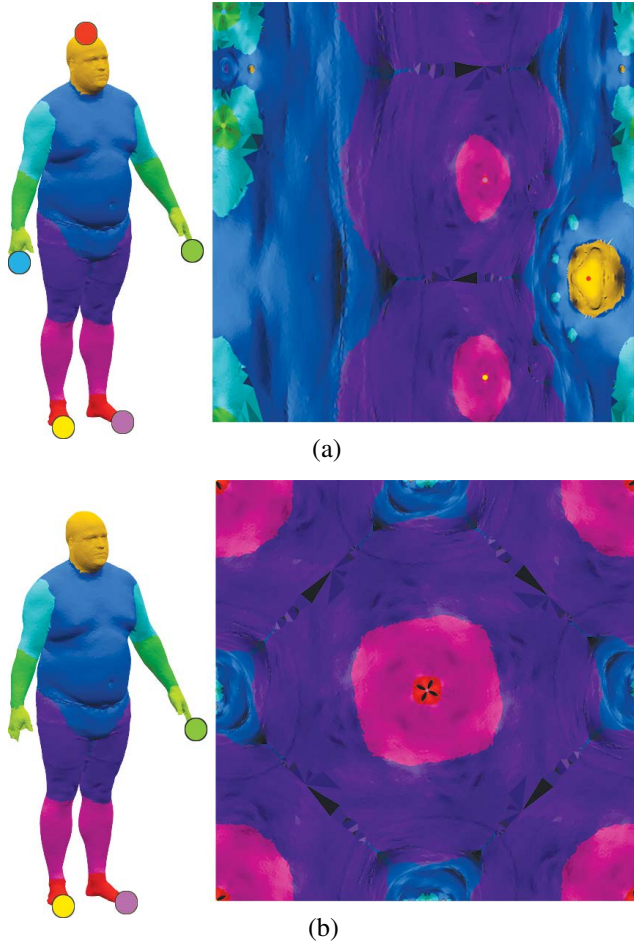


Figure 1. (a) A periodic general cover with 5 branch points (colored disks) and degree $d = 5$ of a human model computed using our method. (b) The orbifold cover of [1] with 3 branch points and degree 4. Note that the cover in (b) has four (rotated) repetitions of the same mapping; is missing a useful scale covering of the head and right arm; and the torso (blue) suffers from a considerable down-scale.

Applying our method to surface learning is easy: One needs to choose one’s desired cover type, transfer whatever input functions on the input surfaces (*e.g.*, x, y, z coordinates) to images and apply one’s favorite CNN with periodic padding. Using this simple procedure on two surface learning tasks, namely semantic surface segmentation, and the SHREC17 shape revrieval benchmark [30] already provided state of the art results. We believe using our surface-to-image representation can become a useful bridge to quickly and effectively transfer successful CNN models to the geometric domain.

2. Previous work

Applying deep learning techniques to geometric data has proved to be a huge success in the last few years. A wide variety of methods were suggested, where the most popular approaches are: volumetric based methods (*e.g.* [37, 21]), rendering based methods(*e.g.* [32, 39]), spectral based methods(*e.g.* [5, 7]) and methods that operate directly on the surface itself (*e.g.* [20]). A popular related problem is the problem of learning on point clouds which received a lot of attention lately (see *e.g.* [27, 2, 17]). Here, we restrict our attention to intrinsic or parameterization-based surface methods and refer the reader to the above mentioned works and a recent survey [4] for further information.

Local parameterization. This class of methods suggests to extract local surface patches, and use them in order to learn point representations [20, 3, 22]. These works differ mainly in the way the patch operator is defined: in [20] the authors use local polar coordinates as the patch operator. In a follow-up work, [3] use projections on oriented anisotropic diffusion kernels, where [22] learn the patch operator using a Gaussian mixture model.

Global parameterization. Another line of work uses global parmeterization of the surface to a canonical domain. [31] use an area-preserving parameterization and maps surfaces to a planar domain (going through a sphere); the global area-preserving parameterization cannot cover the surface with low distortion everywhere and depends on the specific cut made on the surface. [19] suggested to glue four copies of the surface into a torus and map it conformally to a flat torus where the convolution is well defined. The map they use is defined by a choice of three points on the surface, and suffers from significant conformal scale distortion. In order to cover each point on the surface reasonably well, the authors sample multiple triplets of points from each surface where each triplet focuses on a different part of the surface. In a follow up work, the authors of [12] use the same parameterization as a surface representation for Generative Adversarial Networks (GANs) [10]. In order to deal with the high conformal distortion of each single parameterization, the authors devise a multi-chart structure and rely on given sparse correspondences between the surfaces.

Convolutions on tangent planes. [35] define convolutions on surfaces by working on the tangent planes. [23] also define the convolutions on tangent planes and relate convolutions on nearby points using parallel transport. [26] define convolutions on surfaces by extending the notion of a signal on a surface into a directional signal and build layers that are equivariant to the choice of reference directions.

Other methods. [38] tackle the shape segmentation problem by a novel architecture that operates on local features (such as normals) and global features (such as distances) and then fuses them together. In [16], the authors propose an improved graph neural network model based on the Dirac operator.

3. Approach

Denote by \mathcal{M} a sphere-type input surface, and by \mathcal{T}_0 the flat torus, *i.e.* the unit square $[0, 1]^2$ with opposite sides identified (periodic boundary conditions). The key component of our approach is the construction of *branched covering maps*. A branched covering $E_0 : \mathcal{T}_0 \rightarrow \mathcal{M}$ is a map such that, excluding a finite set of points $b_1, \dots, b_n \in \mathcal{M}$, every point in \mathcal{M} has d preimages with homeomorphic neighborhoods². Intuitively, we can think that \mathcal{T}_0 covers \mathcal{M} d times. Figure 2 (a) shows how a branched covering might look for a neighborhood of a branch point b_i .

We use these covering maps to pull data (*i.e.*, functions) $f : \mathcal{M} \rightarrow \mathbb{R}$ from the surface \mathcal{M} to the flat torus \mathcal{T}_0 via

$$f_0 = f \circ E_0. \quad (1)$$

We create (periodic) image representations of surfaces by using this equation to pull the surface functions (*e.g.*, x, y, z coordinates) to \mathcal{T}_0 . These image representations will be useful for learning if E_0 covers well \mathcal{M} . Namely, every part of the surface \mathcal{M} has a preimage on \mathcal{T}_0 with low isometric (*i.e.*, angle and scale) distortion. Note that this definition is a *relaxation* of the usual bijective mapping requirement since it allows each part of the surface to be covered several times. This provides branched coverings sufficient flexibility to represent complex geometry as a single image with low-distortion. For example, Figure 1 (a) shows a degree 5 branched covering with 5 branch points (*i.e.*, each point except of the branch points is covered 5 times). The square image shows a function f over the surface pulled to the flat torus via $f \circ E_0$, as in Equation (1) (in this case f represents semantic segmentation of the human body).

The cover E_0 is constructed as a composition

$$E_0 = E \circ \Phi, \quad (2)$$

where $E : \mathcal{T} \rightarrow \mathcal{M}$ is a branched cover of \mathcal{M} constructed by stitching $d > 1$ copies of the surface \mathcal{M} to create a topological torus \mathcal{T} ; and $\Phi : \mathcal{T}_0 \rightarrow \mathcal{T}$ is a bijective map taking the flat torus to the torus \mathcal{T} . In the following we will detail how to compute E and Φ .

²Formally, A branched cover $E_0 : \mathcal{T}_0 \rightarrow \mathcal{M}$ is characterized by the property that every point in \mathcal{M} , except possibly a finite set of *branch points* $\{b_i\}_{i=1}^n \subset \mathcal{M}$, has a neighborhood, the preimage of which is a disjoint union of neighborhoods in \mathcal{T}_0 so that the restriction of E_0 to each one is a homeomorphism.

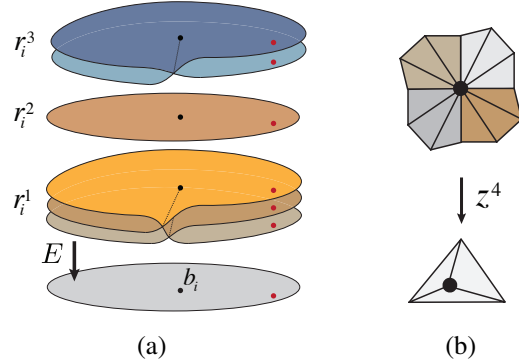


Figure 2. (a) Branched cover over a branch point b_i with ramification $\rho_i = [3, 1, 2]$. (b) Shows an example of mesh ramification of order 4; see RH formula in the text for more details.

3.1. Computing the branched cover $E : \mathcal{T} \rightarrow \mathcal{M}$

Given a covering map $E : \mathcal{T} \rightarrow \mathcal{M}$, each branch point b_i has a ramification structure of the form $\rho_i = [r_i^1, r_i^2, \dots, r_i^{k_i}]$. Here k_i is the number of preimages of b_i , and locally, in the neighborhood of each preimage the cover looks like the complex power function $z \mapsto z^{r_i^k}$; Figure 2 (a) demonstrates the behavior of a covering near a branch point b_i with 3 preimages and ramification structure $\rho_i = [2, 1, 3]$ (black dots). Note that a generic point (red dots) has 6 preimages and trivial ramification structure $\rho_i = [1, 1, 1, 1, 1, 1]$ ³.

The collection of ramification structures over all branch points is the ramification structure of the covering, which we will denote by $\rho = [\rho_1, \dots, \rho_n]$. We define the *degree* of the ramification ρ to be the sum of the elements in a ramification structure defined over any point. By Proposition 7 in [8], the degree is well defined. That is, does not depend on a choice of point. Note that the degree is also the number of preimages of a generic point. We thus have that the ramification indices of ρ_i satisfy

$$\sum_k r_i^k = d. \quad (3)$$

See for example the red dots in Figure 2; there are 6 preimages to the red dot at the bottom, which is exactly the degree of this cover. Another necessary condition for ρ , stems from the so-called Riemann-Hurwitz (RH) formula, (see Proposition 19 in [8]): $\chi(\mathcal{T}) = d \cdot \chi(\mathcal{M}) + \sum_{i,k} (1 - r_i^k)$, where χ is the Euler characteristic. In our case $\chi(\mathcal{T}) = 0$, $\chi(\mathcal{M}) = 2$. Therefore

$$2d = \sum_{i,k} (r_i^k - 1). \quad (4)$$

Intuitively, the RH formula computes the difference between the Euler characteristic of the covering surface \mathcal{T} and covered surface \mathcal{M} ; as an illustrative simple example, Figure

³It is common practice to refer only to ramification structures of branch points.

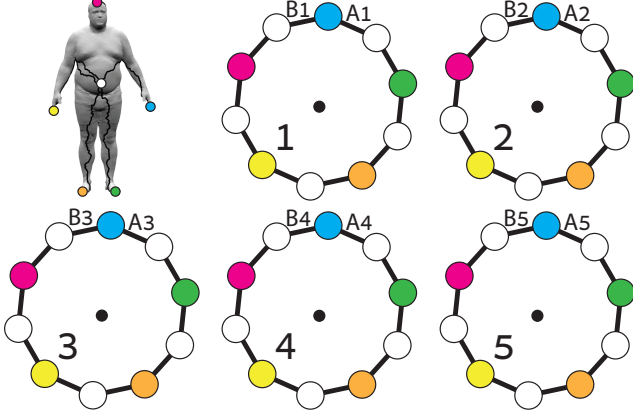


Figure 3. Illustration of the mesh cutting (top-left), and the gluing algorithm. Branch points are visualized as colored disks.

2(b) shows ramification of order 4 and degree 4. RH formula asserts that the Euler characteristic of the top mesh should be 4 times that of the bottom mesh minus 3, which is indeed the case. The subtraction compensates the fact that the center vertex (black dot) is not duplicated.

We next answer the question: Given a set of branch points $b_i \in \mathcal{M}$, $i \in [n]$, solution ρ to (3)-(4), how to practically construct a covering $E : \mathcal{T} \rightarrow \mathcal{M}$? To that end we devise an algorithm that consists the following parts: (i) Cut \mathcal{M} through the branch points to get disk-type version \mathcal{M}' of \mathcal{M} . Duplicate \mathcal{M}' d times. (ii) Compute *gluing instructions* to construct \mathcal{T} from the d copies of \mathcal{M}' . Construct \mathcal{T} by gluing the copies of \mathcal{M}' following the gluing instructions.

Part (i): We represent our surface \mathcal{M} as a triangular mesh $\mathcal{M} = (\mathcal{V}, \mathcal{E}, \mathcal{F})$, with vertex set $\mathcal{V} = \{v_i\}$, edge set $\mathcal{E} = \{e_{ij}\}$, and face set $\mathcal{F} = \{f_{ijk}\}$. The branch points b_i are chosen from the vertex set \mathcal{V} . Part (i) of the algorithm is cutting \mathcal{M} to a disk topology, such that after the cut the branch points are on the boundary. As shown in Figure 3 (top-left) we cut the mesh sequentially along n (in this case $n = 5$) paths from a generic vertex $p \in \mathcal{V}$ (white dot) to each of the branch points b_i (colored dots) making sure the branch points appear on the boundary of \mathcal{M}' . Topologically, \mathcal{M}' is now a disk. Next, we duplicate \mathcal{M}' d times, making copies $\mathcal{M}'_1, \dots, \mathcal{M}'_d$. Figure 3 shows this for $d = 5$. For each $v \in \mathcal{V}'_j$ (vertex of \mathcal{M}'_j) we denote

$$\pi(v) \in \mathcal{V} \quad (5)$$

to be its origin vertex in \mathcal{M} .

Part (ii): We compute gluing instructions to glue the copies \mathcal{M}'_j , $j \in [d]$ to give a torus \mathcal{T} . Mathematically, the gluing instructions come in the form of a set of permutations $\Sigma = \{\sigma_i\}_{i=1}^n$ of $[d]$. The way a permutation σ_i is used to stitch copies \mathcal{M}'_j is illustrated in Figure 3: Consider b_i

(e.g., the blue dots); denote the two boundary edges emanating from b_i by $A_j^{(i)}$ and $B_j^{(i)}$. Each $A_j^{(i)}$ can be stitched to any $B_j^{(i)}$, $j \in [d]$. The permutation σ_i makes a specific choice: $A_j^{(i)}$ is stitched to $B_{\sigma_i(j)}^{(i)}$. Algorithm 1 summarizes the gluing procedure. Finally, our cover map $E : \mathcal{T} \rightarrow \mathcal{M}$ is defined by $E(v) = \pi(v)$, which is well defined over \mathcal{T} .

Data: cut mesh copies \mathcal{M}'_j , $j \in [d]$;
gluing instructions $\Sigma = \{\sigma_i\}$, $i \in [n]$

Result: The torus \mathcal{T} and a branched cover
 $E : \mathcal{T} \rightarrow \mathcal{M}$ with ramification ρ

for every branch point b_i , $i \in [n]$ do

for every copy $j \in [d]$ do

stitch $A_j^{(i)}$ and $B_{\sigma_i(j)}^{(i)}$

end

end

$E : \mathcal{T} \rightarrow \mathcal{M}$ is defined by $E(v) = \pi(v)$, see (5).

Algorithm 1: Gluing algorithm.

Next, we show how to compute the gluing instructions $\Sigma = \{\sigma_i\}_{i=1}^n$ matching a given ramification structure ρ . There are several necessary and sufficient conditions Σ should satisfy:

Lemma 1. *Gluing instructions $\Sigma = \{\sigma_i\}_{i=1}^n$ for prescribed ramification ρ has to satisfy:*

- (i) *The cycle structure of σ_i is $\rho_i = [r_i^1, \dots, r_i^{k_i}]$, $i \in [n]$.*
- (ii) *Σ is a product one tuple, namely $\sigma_1 \cdot \sigma_2 \cdots \sigma_n = Id$.*
- (iii) *The group G generated by Σ is transitive on $[d]$. That is, for each $i, j \in [d]$ there exists $\sigma \in G$ so that $j = \sigma(i)$.*

In the other direction, Σ satisfying (i)-(iii) furnishes valid gluing instructions with ramification ρ .

We prove this theorem in Section 7 and provide an algorithm (Algorithm 2) to compute gluing instructions given ramification ρ . We note that theoretically not all ρ satisfying (3)-(4) have gluing instructions and consequently the desired cover. Nevertheless it is rare to find such examples in practice. In this paper we used ramification structures of the form $\rho = [[1^r, s]^n]$, where 1^r means r times 1 and $[*]^n$ means n identical ramifications for n branch points.

For example, Figure 1 (a) depicts the case $n = 5$, $r = 3$, $s = 2$, namely $[[1, 1, 3]^5]$; every branch point b_i has three preimages, two of which are with no ramification and one with order-3 ramification. The gluing instructions in this case, computed using Algorithm 2, are: $\Sigma = \{(1)(2)(345), (1)(4)(235), (3)(4)(152), (3)(4)(125)\}$.

Note that each of these permutation (ii)-(iii) can be checked as-well. These gluing instructions are used on the copies \mathcal{M}'_j as shown in Figure 3 and described in Algorithm 1 to generate the cover $E : \mathcal{T} \rightarrow \mathcal{M}$ used in Figure 1.

3.2. Computing the map $\Phi : \mathcal{T}_0 \rightarrow \mathcal{T}$

To compute our final cover map $E_0 : \mathcal{T}_0 \rightarrow \mathcal{M}$ we need to compute a low distortion flattening $\Phi : \mathcal{T}_0 \rightarrow \mathcal{T}$, see Equation (2). We equivalently compute $\Phi^{-1} : \mathcal{T} \rightarrow \mathcal{T}_0$ where \mathcal{T} is represented as a mesh constructed in the previous section, $\mathcal{T} = (\mathcal{V}_{\mathcal{T}}, \mathcal{E}_{\mathcal{T}}, \mathcal{F}_{\mathcal{T}})$. We use a version of the orbifold Tutte embedding described in [1] to compute as conformal as possible harmonic map $\mathcal{T} \rightarrow \mathcal{T}_0$.

Explicitly, we cut \mathcal{T} along its two basic loops l_1, l_2 to a disk-like surface \mathcal{T}' . Denote by $v_0 \in \mathcal{V}_{\mathcal{T}'}$ the origin of both loops. We find the loops using Algorithm 5 in [14]. Next we solve a Laplacian-like linear system $AF = b$, where $A \in \mathbb{R}^{m \times m}$, $m = |\mathcal{V}_{\mathcal{T}'}|$ (number of vertices in the cut torus \mathcal{T}'), $F \in \mathbb{R}^{m \times 2}$ represents a piecewise linear map Φ^{-1} by prescribing the images on the plane of the vertices $\mathcal{V}_{\mathcal{T}'}$, i.e., $F_v \in \mathbb{R}^2$ is the planar image of the vertex $v \in \mathcal{V}_{\mathcal{T}'}$. The matrix A and vector b are set as follows: (i) The 4 preimages of v_0 in \mathcal{T}' are mapped to the corner of the unit square $[0, 1]^2$. (ii) The two preimages of l_1 are mapped to the plane so their difference is a constant translation of $(1, 0)$; similarly for l_2 the difference is set to be the constant translation of $(0, 1)$. (iii) All the remaining vertices of \mathcal{T}' are mapped to the plane so that they satisfy the convex combination property w.r.t. their neighbors (the discrete harmonic definition): $\sum_{u \in N_v} w_{vu} (F_v - F_u) = 0$, where N_v is the set of vertices in \mathcal{T}' adjacent to v and w_{uv} are the cotangent weights [25]. The resulting map is discrete harmonic [18], approximately conformal up to a constant affine transformation, and as proven in [1] the piecewise linear function defined by F is indeed a bijection $\Phi^{-1} : \mathcal{T} \rightarrow \mathcal{T}_0$. We finally have all pieces in place to compute E_0 as defined in (2).

4. Implementation Details

Data generation. We used two covering types in the experiments below: for surface segmentation we opted for $\rho_i = [5, 1^5]$, $i \in [n]$, $n = 5$; and for shape retrieval (i.e., learning functions over the sphere) $\rho_i = [2, 1]$, $i \in [n]$, $n = 6$. The motivation in choosing those ramification structures is two-fold: we want all branch points to be treated equally by the cover, and applying higher ramification order improve shrinking of protruding parts. We used Algorithm 2 to compute the gluing instructions in each case. We generate images from surface functions by using E_0 (see Equation (2)) to push a piecewise linear function over the surface to a piecewise linear function over a triangulation of \mathcal{T}_0 and sample it at a regular grid using bilinear interpolation. For the surface segmentation task, we choose the 5 branch points to be the top 5 local maxima of the Average Geodesic Descriptor (AGD) [15] on the surface. We also find the minimal AGD point and use it as the base point for cutting the mesh. We use the shortest paths from this base point to all branch points in order to cut the mesh; when the mesh does not

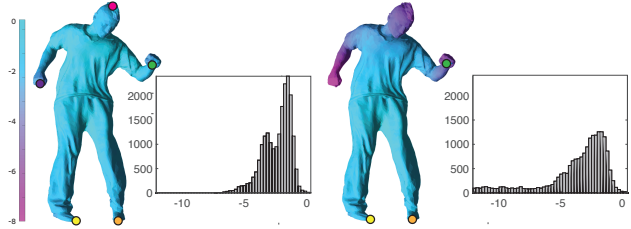


Figure 4. Area scaling (the histogram is in log scale) of our method (left) and orbifold cover [19] (right). Note that the orbifold cover shrinks large parts of the surface considerably.

allow such a path we subdivide it locally (without changing its geometry). For spherical data learning we took 6 branch points on the sphere using farthest point sampling. This pre-processing step was implemented in Matlab. It takes ~ 22 seconds in average to generate a periodic (toric) image for a mesh with 6890 vertices on a single CPU core in an Intel(R) Xeon(R) CPU E5-2670 v3 @ 2.30GHz machine.

Learning. We use Pytorch [24] for learning. In the experiments we use off-the-shelf CNN models with just one small tweak: we replaced the standard zero padding with periodic padding.

Prediction. In case the network outputs per-pixel labels, e.g., in a segmentation task, we pull the labels back to the surface in the following way: First, transfer the per-pixel logits to the faces $\mathcal{F}_{\mathcal{T}}$ of the toric mesh using bilinear interpolation sampled at the faces' centers. Second, each face f_{ijk} in \mathcal{M} has d corresponding faces in the toric mesh \mathcal{T} . We set the label of f_{ijk} according to the max entry of the weighted logits. We take the area scale of triangles to be the weight, that is, better scaled triangles receive more weight in the average.

5. Experiments

5.1. Cover evaluation

We compare the scale distortion caused by our method using the $[5, 1^5]^5$ ramification structure and the orbifold covering of [19]. Figure 4 shows the area distortion using our cover with 5 branch points and the orbifold cover with the first 3 branch points. An orbifold covering can only allow a small number of branch points with a very particular ramification structure. In fact [1], there are only four options: $[[2][2][2][2]]$, $[[3][3][3]]$, $[[4][4][22]]$, $[[222][33][6]]$. Lack of high ramification order and larger number of branch points creates extreme shrinking effects. As can be seen in the histogram, as well as in the color coded scale function over the surface, our method does not scale much surface area below 10^{-5} . However, the orbifold covering shrinks significant

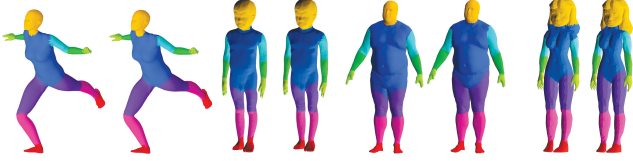


Figure 5. Four segmentation results of our method. In each pair: left is our result and right is ground truth.

parts of the surface (*i.e.*, head and two arms) considerably. Lastly, note that the orbifold covering is symmetric and repeats the same covering several times. Therefore, it is suboptimal in utilizing the image resolution.

5.2. Surface segmentation

We use the human segmentation benchmark from [19] that consists of 373 train models from multiple sources and 18 test models. 5% randomly sampled train models were used as a validation set (18 models). All models are given as triangular meshes. For each model, each face is labeled according to a predefined partition of the human body (*e.g.* head, torso, hands, etc.). The task is to label faces of new unseen human models with these labels. For each model we generated an augmented set of 100 images per mesh, by permuting the order of the branch points, multiplying the vertices by a random orthogonal matrix and a uniform scale sampled from [0.85, 1.15] as suggested in [26]. We use a similar augmentation of 10 images per mesh in the test set, and predict each face on the original mesh using a majority vote.

Table 1 summarizes the results of this experiment, where our method outperformed the compared methods; Figure 5 shows typical segmentation results. Our method achieves state of the art results compared to the following methods: Geodesic Convolutions [20], Toric CNN [19], pointnet++ [28], dynamic graph CNN [36], and the recent multi-directional geodesic convolution method[26].

For this application we used the U-net architecture [29] with 16 layers, with the following feature-channels sizes: $3 - 128^4 - MP - 128 - MP - 256 - MP - 512 - MP - 512 - MP - 256 - UP - (128 - MP)^4 - 8$, where $MP = \text{max pooling}$ and $UP = \text{upsampling}$ with nearest-neighbour interpolation. Kernel sizes are 5 for the first layer, 1 for the last layer, and 3 for all other layers. After each convolution we use *ReLU* with a Batch-Normalization layer [13]. We used a weighted loss with equal probability labels, and trained the network using stochastic gradient descent with momentum [33] for 40 epochs with learning rate 0.2, batch size 2, and learning rate decay of 0.995. Training takes ~ 3 hours per epoch on a Tesla P100-PCIE-16GB Nvidia GPU.

Table 1. Comparison of results on the human segmentation benchmark from [19].

method	Inputs	accuracy
Toric CNN.	WKS,AGD,curv	88.00%
Geodesic Conv	3D coords	76.49%
Pointnet++	3D coords	90.77%
Dynamic graph CNN	3D coords	89.72%
Multi-directional Conv.	3D coords	88.61%
Ours	3D coords	91.02%

5.3. 3D shape retrieval

We tested our framework for 3D model retrieval using the SHREC2017 benchmark [30]. This dataset contains 51162 3D models from 55 different categories. The benchmark provides (70%, 20%, 10%) train/validation/test split. There are two separate challenges: (i) the shapes are consistently aligned (ii) the shapes are randomly rotated. We tackle the (harder) second challenge. Since the shapes are not of genus zero we follow the protocol of [6] that projected the meshes on a bounding sphere using ray casting, and recorded six functions on this sphere: distance to the model, \cos/\sin of the model angles (this is done for both the model and its convex-hull). We then use our method in order to flatten the sphere and map these spherical signals to the periodic images (flat torus).

We compared our method to the top methods in each category, the Spherical CNN method [6], and the recent [9]. The results are presented in Table 2; note that in the F1 measure we scored first among all methods. For this application we used a slight modification of the inception v3 architecture [34]. We trained the network for 100 epochs with learning rate 0.1, batch size of 32, and learning rate decay of 0.995. Training took 30 minutes per epoch on a Tesla P100-PCIE-16GB Nvidia GPU.

6. Conclusions

In this paper, we introduced a new method for representing sphere-type surfaces as toric images that can be used in standard Convolutional Neural Network framework for shape learning tasks. The method allows faithful representation of *all parts of the surface*, thus alleviating the need to generate multiple maps to cover each surface. Practically, we showed that off-the-shelf CNN models applied to images generated with our method already lead to state of the art performance in the tasks of surface segmentation and retrieval.

The main limitation of this work is its restriction to genus zero surfaces. This kind of models are abundant, but certainly do not exhaust all 3D models. We would like to seek a generalization of this method to point clouds and depth images as-well as more general topological types. One sim-

Table 2. Comparison of our method and the top results in each category on the SHREC17 benchmark [30]

	P@N	R@N	F1@N	mAP	NDCG
FURUYA_DLAN	0.814	0.683	0.706	0.656	0.754
Tatsuma_ReVGG	0.705	0.769	0.719	0.696	0.783
SHREC16-Bai_GIFT	0.678	0.667	0.661	0.607	0.735
Deng_CM-VGG-6DB	0.412	0.706	0.472	0.524	0.642
Spherical CNN [6]	0.701	0.711	0.699	0.676	0.756
SO(3) Equivariant Representations CNNs[9]	0.717	0.737	-	0.685	-
Ours	0.746 (2 nd)	0.740 (2 nd)	0.737 (1 st)	0.710 (1 st)	0.790 (1 st)

ple thing to try is to use sphere-type surface to approximate general surfaces. Another interesting future work direction is to seek other shape learning tasks that can benefit from these image representations.

7. Proofs and computing gluing instructions

In this section we prove Lemma 1 and describe an algorithm that finds tuples of permutations $\sigma_1, \dots, \sigma_n \in S_d$, corresponding to a prescribed ramification structure ρ , up to simultaneous conjugation. We call such a tuple a product one tuple. We implement our algorithm using Magma computational algebra system [11].

We recall the following topological facts. A degree d branched covering map $E : \mathcal{T} \rightarrow \mathcal{M}$ induces a group homomorphism, called the monodromy representation, from π_1 , the fundamental group of $\mathcal{M} \setminus \{b_1, \dots, b_n\}$ to S_d .

The homomorphism is given as follows: We take each loop $l \in \pi_1$, based at a point p , and lift it to \mathcal{T} starting from a preimage of p . This lift has to end at another preimage of p . Due to properties of the lifting, this induces a permutation on the preimages of p in \mathcal{T} , referred to as the *fiber* of p .

The group π_1 has n generators and a single relation. The generators, l_1, \dots, l_n , are the n loops around each of the branch points. The relation is $l_1 * \dots * l_n = 1$.

Our gluing instructions, $\sigma_1, \dots, \sigma_n$, will be the images of l_1, \dots, l_n under the monodromy representation.

Proof of Lemma 1. First we prove that the conditions in the lemma are necessary.

For (i), we note that a lift of a loop around a branch point l_i with a particular cycle structure induces a permutation with the same cycle structure.

For (ii), the fact that $l_1 * \dots * l_n = 1$, implies (using group homomorphism) that $\sigma_1 \cdot \dots \cdot \sigma_n = I_d$.

For (iii), fix p_1, p_2 in the fiber of p . Since \mathcal{T} is connected, there exists a path γ connecting p_1 and p_2 . The loop $E \circ \gamma$ is a loop starting and ending at p whose lift takes p_1 to p_2 . Thus, the action of group generated by $\Sigma = \{\sigma_1, \dots, \sigma_n\}$ is transitive.

The fact that these conditions are sufficient is called Riemann's existence theorem (RET). See Theorem 2, page 49 in [8]. \square

We now describe our algorithm to find gluing instructions with prescribed ramification structure ρ . We denote the conjugacy class in S_d associated with the cycle structure of ρ_i by C_i . In the algorithm construction we use the following:

Claim 1. (i) $\langle \sigma_1, \sigma_2, \dots, \sigma_{n-1} \rangle$ is a transitive permutation group and $\prod_{i=1}^{n-1} \sigma_i \in C_n$, if and only if $\sigma_1, \sigma_2, \dots, \sigma_n$, where $\sigma_n = (\sigma_1 \sigma_2 \dots \sigma_{n-1})^{-1}$ is a transitive product one tuple with $\sigma_n \in C_n$.

(ii) The set $\{\sigma_1, \dots, \sigma_i\}$ can be completed to a transitive product one tuple compatible with a ramification structure ρ if and only if $\{\sigma_1, \dots, \sigma_{i-1}, g\sigma_i g^{-1}\}$, for any $g \in Z(\sigma_1, \dots, \sigma_{i-1})$ (Z denote the centralizer), can be completed to a transitive product one tuple compatible with ρ .

Proof. (i) follows from the observations that adding elements to a transitive generator set keeps the set transitive, and that the cycle structure of g and g^{-1} is the same. For (ii), note that for any $g \in Z(\sigma_1, \dots, \sigma_{i-1})$ and $j \in [i-1]$ it holds that $g\sigma_j g^{-1} = \sigma_j$. Thus, for any $g \in Z(\sigma_1, \dots, \sigma_{i-1})$, we have that any tuple with $\sigma_1, \dots, \sigma_i$ is the same as a tuple with $g\sigma_1 g^{-1}, \dots, g\sigma_i g^{-1}$, up to simultaneous conjugation. \square

The main idea in the algorithm for finding all gluing instructions corresponding to a ramification type ρ is to exhaustively go over all tuples $\sigma_i \in C_i$ and check whether they form a product one tuple. We use the claim above to prune this exhaustive search, as described in Algorithm 2. Note that this computation is done once for a given cover ramification type and is reused for all models using this type of cover.

References

- [1] N. Aigerman and Y. Lipman. Orbifold tutte embeddings. *ACM Trans. Graph.*, 34(6):190–1, 2015. 2, 5
- [2] M. Atzmon, H. Maron, and Y. Lipman. Point convolutional neural networks by extension operators. *ACM Trans. Graph.*, 37(4):71:1–71:12, July 2018. 2
- [3] D. Boscaini, J. Masci, E. Rodolà, and M. Bronstein. Learning shape correspondence with anisotropic convolutional neural

Data: a ramification structure $\rho = (\rho_1, \dots, \rho_n)$
Result: all gluing instructions Σ compatible with ρ
 Pick $\sigma_1 \in C_1$
 Call the recursive function **tuplesFinder**(ρ, σ_1)

```

tuplesFinder( $\rho, \{\sigma_1, \dots, \sigma_i\}$ )
while  $C_i \neq \emptyset$  do
  pick  $\sigma_i \in C_i$ 
  update  $C_i = C_i \setminus$ 
     $Z(\sigma_1, \sigma_2, \dots, \sigma_{i-1})\sigma_i Z(\sigma_1, \sigma_2, \dots, \sigma_{i-1})^{-1}$ 
  if  $i = n - 1$  then
    if  $\prod_{i=1}^{n-1} \sigma_i$  and  $\sigma_n$  are conjugates and
       $\langle \sigma_1, \sigma_2, \dots, \sigma_{n-1} \rangle$  is transitive then
        add  $\sigma_1, \sigma_2, \dots, \sigma_n$  to list of product one
        tuples
      end
    end
  else
    call tuplesFinder( $\rho, \{\sigma_1, \sigma_2, \dots, \sigma_i\}$ )
  end
end

```

Algorithm 2: Finding gluing instructions.

networks. In *Advances in Neural Information Processing Systems*, pages 3189–3197, 2016. 2

- [4] M. M. Bronstein, J. Bruna, Y. LeCun, A. Szlam, and P. Vandergheynst. Geometric deep learning: going beyond euclidean data. *IEEE Signal Processing Magazine*, 34(4):18–42, 2017. 2
- [5] J. Bruna, W. Zaremba, A. Szlam, and Y. LeCun. Spectral networks and locally connected networks on graphs. *arXiv preprint arXiv:1312.6203*, 2013. 2
- [6] T. S. Cohen, M. Geiger, J. Köhler, and M. Welling. Spherical cnns. *arXiv preprint arXiv:1801.10130*, 2018. 6, 7
- [7] M. Defferrard, X. Bresson, and P. Vandergheynst. Convolutional neural networks on graphs with fast localized spectral filtering. In *Advances in Neural Information Processing Systems*, pages 3844–3852, 2016. 2
- [8] S. Donaldson. *Riemann surfaces*. Oxford University Press, 2011. 3, 7
- [9] C. Esteves, C. Allen-Blanchette, A. Makadia, and K. Daniilidis. Learning so (3) equivariant representations with spherical cnns. In *Proceedings of the European Conference on Computer Vision (ECCV)*, pages 52–68, 2018. 6, 7
- [10] I. Goodfellow, J. Pouget-Abadie, M. Mirza, B. Xu, D. Warde-Farley, S. Ozair, A. Courville, and Y. Bengio. Generative adversarial nets. In *Advances in neural information processing systems*, pages 2672–2680, 2014. 2
- [11] M. Group et al. Magma computational algebra system, version 2.22-7, sydney. 2016. 7
- [12] H. B. Hamu, H. Maron, I. Kezurer, G. Avineri, and Y. Lipman. Multi-chart generative surface modeling. *arXiv preprint arXiv:1806.02143*, 2018. 2
- [13] S. Ioffe and C. Szegedy. Batch normalization: Accelerating deep network training by reducing internal covariate shift. *arXiv preprint arXiv:1502.03167*, 2015. 6
- [14] M. Jin, X. Gu, Y. He, and Y. Wang. *Conformal Geometry: Computational Algorithms and Engineering Applications*. Springer, 2018. 5
- [15] V. G. Kim, Y. Lipman, and T. Funkhouser. Blended intrinsic maps. In *ACM Transactions on Graphics (TOG)*, volume 30, page 79. ACM, 2011. 5
- [16] I. Kostrikov, Z. Jiang, D. Panozzo, D. Zorin, and J. Bruna. Surface networks. In *The IEEE Conference on Computer Vision and Pattern Recognition (CVPR)(June 2018)*, volume 3, 2017. 3
- [17] Y. Li, R. Bu, M. Sun, and B. Chen. Pointcnn. *arXiv preprint arXiv:1801.07791*, 2018. 2
- [18] L. Lovász. Discrete analytic functions: an exposition. *Surveys in differential geometry*, 9(1):241–273, 2004. 5
- [19] H. Maron, M. Galun, N. Aigerman, M. Trope, N. Dym, E. Yumer, V. G. Kim, and Y. Lipman. Convolutional neural networks on surfaces via seamless toric covers. *ACM Trans. Graph*, 36(4):71, 2017. 1, 2, 5, 6
- [20] J. Masci, D. Boscaini, M. Bronstein, and P. Vandergheynst. Geodesic convolutional neural networks on riemannian manifolds. In *Proceedings of the IEEE international conference on computer vision workshops*, pages 37–45, 2015. 1, 2, 6
- [21] D. Maturana and S. Scherer. Voxnet: A 3d convolutional neural network for real-time object recognition. In *Intelligent Robots and Systems (IROS), 2015 IEEE/RSJ International Conference on*, pages 922–928. IEEE, 2015. 1, 2
- [22] F. Monti, D. Boscaini, J. Masci, E. Rodola, J. Svoboda, and M. M. Bronstein. Geometric deep learning on graphs and manifolds using mixture model cnns. In *Proc. CVPR*, volume 1, page 3, 2017. 2
- [23] H. Pan, S. Liu, Y. Liu, and X. Tong. Convolutional neural networks on 3d surfaces using parallel frames. *arXiv preprint arXiv:1808.04952*, 2018. 2
- [24] A. Paszke, S. Gross, S. Chintala, G. Chanan, E. Yang, Z. DeVito, Z. Lin, A. Desmaison, L. Antiga, and A. Lerer. Automatic differentiation in pytorch. 2017. 5
- [25] U. Pinkall and K. Polthier. Computing discrete minimal surfaces and their conjugates. *Experimental mathematics*, 2(1):15–36, 1993. 5
- [26] A. Poulencard and M. Ovsjanikov. Multi-directional geodesic neural networks via equivariant convolution. *arXiv preprint arXiv:1810.02303*, 2018. 2, 6
- [27] C. R. Qi, H. Su, K. Mo, and L. J. Guibas. Pointnet: Deep learning on point sets for 3d classification and segmentation. *Proc. Computer Vision and Pattern Recognition (CVPR), IEEE*, 1(2):4, 2017. 1, 2
- [28] C. R. Qi, L. Yi, H. Su, and L. J. Guibas. Pointnet++: Deep hierarchical feature learning on point sets in a metric space. In *Advances in Neural Information Processing Systems*, pages 5099–5108, 2017. 1, 6
- [29] O. Ronneberger, P. Fischer, and T. Brox. U-net: Convolutional networks for biomedical image segmentation. In *International Conference on Medical image computing and computer-assisted intervention*, pages 234–241. Springer, 2015. 6
- [30] M. Savva, F. Yu, H. Su, A. Kanezaki, T. Furuya, R. Ohbuchi, Z. Zhou, R. Yu, S. Bai, X. Bai, et al. Shrec’17 track large-scale 3d shape retrieval from shapenet core55. 2, 6, 7

- [31] A. Sinha, J. Bai, and K. Ramani. Deep learning 3d shape surfaces using geometry images. In *European Conference on Computer Vision*, pages 223–240. Springer, 2016. [1](#), [2](#)
- [32] H. Su, S. Maji, E. Kalogerakis, and E. Learned-Miller. Multi-view convolutional neural networks for 3d shape recognition. In *Proceedings of the IEEE international conference on computer vision*, pages 945–953, 2015. [1](#), [2](#)
- [33] I. Sutskever, J. Martens, G. Dahl, and G. Hinton. On the importance of initialization and momentum in deep learning. In *International conference on machine learning*, pages 1139–1147, 2013. [6](#)
- [34] C. Szegedy, V. Vanhoucke, S. Ioffe, J. Shlens, and Z. Wojna. Rethinking the inception architecture for computer vision. In *Proceedings of the IEEE conference on computer vision and pattern recognition*, pages 2818–2826, 2016. [6](#)
- [35] M. Tatarchenko, J. Park, V. Koltun, and Q.-Y. Zhou. Tangent convolutions for dense prediction in 3d. In *Proceedings of the IEEE Conference on Computer Vision and Pattern Recognition*, pages 3887–3896, 2018. [2](#)
- [36] Y. Wang, Y. Sun, Z. Liu, S. E. Sarma, M. M. Bronstein, and J. M. Solomon. Dynamic graph cnn for learning on point clouds. *arXiv preprint arXiv:1801.07829*, 2018. [6](#)
- [37] Z. Wu, S. Song, A. Khosla, F. Yu, L. Zhang, X. Tang, and J. Xiao. 3d shapenets: A deep representation for volumetric shapes. In *Proceedings of the IEEE conference on computer vision and pattern recognition*, pages 1912–1920, 2015. [1](#), [2](#)
- [38] H. Xu, M. Dong, and Z. Zhong. Directionally convolutional networks for 3d shape segmentation. In *Proceedings of the IEEE International Conference on Computer Vision*, pages 2698–2707, 2017. [3](#)
- [39] T. Yu, J. Meng, and J. Yuan. Multi-view harmonized bilinear network for 3d object recognition. In *Proceedings of the IEEE Conference on Computer Vision and Pattern Recognition*, pages 186–194, 2018. [2](#)